Associated production of Higgs boson and $t\bar{t}$ at LHC*

Hong-Lei Li(李洪蕾)[1;1)] Peng-Cheng Lu(路鹏程)[2,1;2)] Zong-Guo Si(司宗国)[2,3;3)] Ying Wang(王英)[2;4)]

[1] School of Physics and Technology, University of Jinan, Jinan Shandong 250022, China
[2] School of Physics, Shandong University, Jinan, Shandong 250100, China
[3] CCEPP, Institute of High Energy Physics, Chinese Academy of Sciences, Beijing 100049, China

Abstract: One of the future goals of the LHC is to precisely measure the properties of the Higgs boson. The associated production of a Higgs boson and top quark pair is a promising process to investigate the related Yukawa interaction and the properties of the Higgs. Compared with the pure scalar sector in the Standard Model, the Higgs sector contains both scalars and pseudoscalars in many new physics models, which makes the $t\bar{t}H$ interaction more complex and provides a variety of phenomena. To investigate the $t\bar{t}H$ interaction and the properties of the Higgs, we study the top quark spin correlation observables at the LHC.

Keywords: Higgs boson, top quark spin correlation, LHC

PACS: 14.80.Ec, 14.65.Ha, 12.60.Fr **DOI:** 10.1088/1674-1137/40/6/063102

1 Introduction

The discovery of the Higgs boson, confirmed by the ATLAS and CMS experiments at the LHC [1, 2], provides forceful evidence for the Brout-Englert-Higgs mechanism in the Standard Model (SM). The impressive accurate experimental results not only support the success of the SM but also push the theoretical predictions forward to a higher accuracy. As well as the mass and spin, other properties of the Higgs boson should be clarified to achieve the completeness of the SM. It is well known that the masses of fermions are extracted from the related Yukawa interactions, which offers the opportunity to study the interaction of the Higgs boson and fermions. Due to the large quark mass, the Yukawa coupling of $t\bar{t}H$ is of the order of one. Therefore many phenomena can be studied in Higgs boson production associated with a top quark pair.

Precise measurements of the Higgs sector are indispensable for an understanding of the origin of electroweak symmetry breaking. The latest results on the Higgs mass as well as the spin and parity [3–6] have been reported by the ATLAS and CMS collaborations. At the same time the couplings of Higgs boson are consistent with the predictions in the SM [4, 7]. However, a Higgs with the same properties could be included in new physics models, such as the Two Higgs Doublet Models [8–10], the Minimal Supersymmetric Models [11-13] and the Left-right Symmetric Models [14–18], etc. The top quark, as the known heaviest quark, is expected to decay before hadronization because of its short lifetime. Hence, its spin property can be transferred to its decay products. The spin effects of $t\bar{t}$ production have been studied at the hadron colliders [19–28]. It is found that the top quark spin effects are sensitive to the new interactions [29–31]. Investigating $t\bar{t}H$ production is helpful to discriminate the Higgs boson among various models. The leading-order and the next-to-leading-order $t\bar{t}H$ cross section predictions have been made in the literature [32–38]. Both the ATLAS and CMS experiments measured $t\bar{t}H$ production with $H\to b\bar{b}$ at $\sqrt{S}=8$ TeV [39, 40]. Some phenomena of the $t\bar{t}H$ interaction have been studied in Refs. [41–47]. The reconstruction of the $t\bar{t}H$ signal and the corresponding background analysis have been studied in detail [48, 79]. The CP-properties of the $t\bar{t}H$ interaction play an important role in the understanding of the Yukawa interaction, which can be probed through Higgs production in association

Received 18 September 2015, Revised 25 January 2016

∗ Supported by National Natural Science Foundation of China(11275114, 11325525 and 11305075) and Natural Science Foundation of Shandong Province (ZR2013AQ006)

1) E-mail: sps_lihl@ujn.edu.cn.cn
2) E-mail: lupcsdu@163.com
3) E-mail: zgsi@sdu.edu.cn
4) E-mail: wang_y@mail.sdu.edu.cn

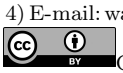

with the top quark pair at the LHC [50–54]. Besides the topics discussed in previous works, in this paper we concentrate on the spin observables with different scalar Higgs masses. Then we discuss systematically the spin observables for the scalar, pseudoscalar and mixing Higgs in $t\bar{t}H$ production at the LHC. Additionally, we investigate simply the corresponding background processes for our signal process $pp \to t\bar{t}H \to b\bar{b}l^+l^-\nu_l\bar{\nu}_l + b\bar{b}$. These results both at LHC 13 TeV and 33 TeV can help to study the Higgs properties.

This paper is organized as follows. The $t\bar{t}H$ interactions in the SM and the Two Higgs Doublet Models are reviewed in Section 2, together with a brief introduction of top quark spin correlations. The $t\bar{t}H$ production at the LHC and the corresponding observables are analyzed in Section 3. Finally, a short summary is given.

2 The $t\bar{t}H$ interaction and the top quark spin effects

In the SM, the scalar sector includes one $SU(2)$ doublet. After spontaneous symmetry breaking, the Higgs boson couples to the top quark according to the formula

$$\mathcal{L}_{t\bar{t}H}(\mathrm{SM}) = -\frac{m_t}{v} t\bar{t}H, \tag{1}$$

where m_t is the top quark mass and v is the vacuum expectation value of the Higgs. Naturally, this interaction is CP-even under CP transformation.

In the Two-Higgs-Doublet Model, there are two $SU(2)$ doublets in the scalar sector. This means there are two vacuum expectation values, v_1 and v_2. Therefore, one generalized representation for the scalar doublet is

$$\Phi_\alpha = \begin{pmatrix} \phi_\alpha^+ \\ (v_\alpha + \rho_\alpha + i\eta_\alpha)/\sqrt{2} \end{pmatrix}, \qquad (\alpha = 1, 2), \tag{2}$$

with $v_1 = v\cos\beta$ and $v_2 = v\sin\beta$ and ϕ_α^+, ρ_α and η_α are the scalar fields. After spontaneous symmetry breaking, there remain five physical Higgs particles: two CP-even H_1 and H_2 bosons, one CP-odd A boson, and two charged $H^\pm$ bosons. Naturally, the light neutral Higgs H_1 could be regarded as the SM Higgs boson. Following that, the Yukawa coupling for the neutral Higgs bosons can be obtained from the Lagrangian

$$\mathcal{L}_{f\bar{f}H} = -\sum_{f=u,d,l} \frac{m_f}{v} (\epsilon^f_{H_1} f\bar{f}H_1 + \epsilon^f_{H_2} f\bar{f}H_2 - i\epsilon^f_A f\gamma_5 \bar{f}A), \tag{3}$$

which brings three types of Yukawa interaction for the SM-like Higgs, the heavy Higgs and the pseudoscalar Higgs respectively. Hence, the $t\bar{t}H$ interaction gets more complicated and leads to different properties for the production.

Because the top quark lifetime is extremely short, it decays without hadronization. Thus the decay production becomes important to analyze the top quark spin information. Defining the angle of the decay particle's (f's) direction of motion with the top quark spin polarization direction as θ, one can obtain the distribution of the decay production by the formula

$$\frac{d\Gamma}{\Gamma d\cos\theta} = \frac{1}{2}(1 + p c_f \cos\theta), \tag{4}$$

where p is the polarization degree, c_f is the spin-analyzer power of f, and f can be l^+, ν, W^+, q, $\bar{q}$. In the SM, the tree level result shows that $c_{l^+} = c_{\bar{d}} = 1$, $c_\nu = c_u = -0.3$, and $c_b = c_{W^+} = -0.39$. Thus the charged lepton and the down type light quark are the best spin analyzers.

In top quark pair production, the spin correlation is related to the final charged lepton. According to the spin correlation, the spin asymmetry of $t\bar{t}$ manifests in the decay particle distribution

$$\begin{aligned} \frac{1}{\sigma}\frac{d\sigma}{d\cos\phi} &= \frac{1}{2}(1 - D\cos\phi), \\ \frac{1}{\sigma}\frac{d\sigma}{d\cos\theta_1 d\cos\theta_2} &= \frac{1}{4}(1 + A_1\cos\theta_1 + A_2\cos\theta_2 \\ &\quad - A_3\cos\theta_1\cos\theta_2), \end{aligned} \tag{5}$$

where σ denotes the cross section of the respective reaction. Here $\phi = \angle(\hat{q}_+ \cdot \hat{q}_-)$, $\theta_1 = \angle(\hat{q}_+ \cdot \hat{a})$ and $\theta_2 = \angle(\hat{q}_- \cdot \hat{b})$ with $\hat{q}_+$ ($\hat{q}_-$) the direction of the lepton l^+ or jet j_1 (l'^- or j_2) from $t(\bar{t})$ decay in the $t(\bar{t})$ rest frame and $\hat{a}$, $\hat{b}$ the reference axes, which can be chosen freely. The coefficient $A_1(A_2)$ reflects the single spin effects in $t\bar{t}$ production and A_3 is a measure of $t\bar{t}$ spin correlations. The polarization and the spin correlation provide important information on the dynamics of the top quark. Similar distributions of $t\bar{t}H$ production at the hadron colliders can be obtained, which supports the investigation of the spin effects in $t\bar{t}H$ production at the LHC.

3 Phenomenology of $t\bar{t}H$ production at the LHC

At the proton-proton colliders $t\bar{t}H$ is produced via the quark annihilation and gluon fusion processes, which are displayed in Fig. 1 at leading order QCD. Because charged leptons are a good trigger for detectors at proton-proton colliders (e.g. the LHC), we investigate the $t\bar{t}H$ production process with both top quarks decaying leptonically,

$$pp \to t\bar{t}H \to bl^+\nu\bar{b}l^-\bar{\nu}H, \quad (l = e, \mu). \tag{6}$$

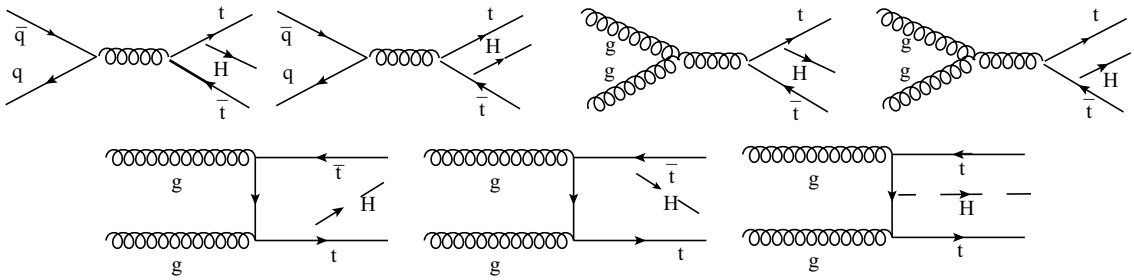

Fig. 1. The Feynman diagrams for $t\bar{t}H$ production at leading order QCD.

From Equation (3), the $t\bar{t}H$ interaction is different for scalar and pseudoscalar Higgs. In the following, we study the $t\bar{t}$ production in association with a light Higgs (SM-Higgs), heavy Higgs and scalar-pseudoscalar mixing Higgs respectively. The top quark mass is set at 173.2 GeV and the SM-Higgs mass is at 125 GeV for the numerical results.

3.1 The SM-Higgs production associated with $t\bar{t}$

The cross section corresponding to process (6) is plotted as a function of center-of-mass energy at a proton-proton collider in Fig. 2. The number of events for $t\bar{t}H$ production with leptonic top quark decay is about 5000 (17000) at LHC 13 TeV with integrated luminosity of 300 (1000) fb^{-1}, and can be up to 20000 (150000) at LHC 14 (33) TeV with integrated luminosity of 1000 fb^{-1}. The cross section can be tuned by a K-factor of 1.2-1.5 from the higher order calculations [34–38].

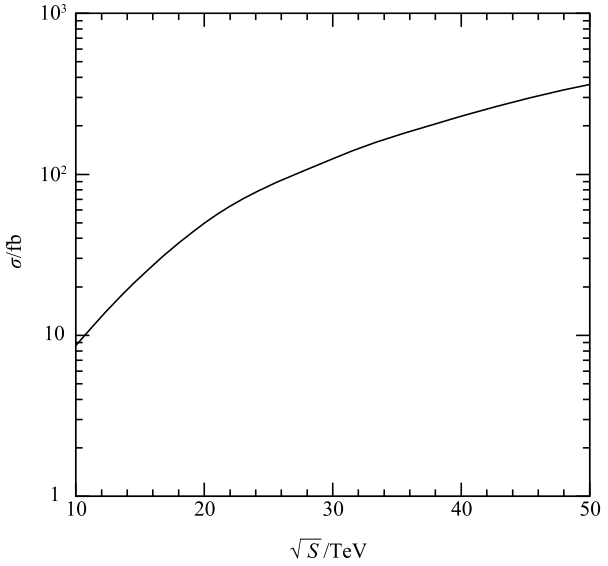

Fig. 2. The cross section for process (6) as a function of center-of-mass energy for SM-Higgs.

According to equation (5), the coupling of $t\bar{t}H$ is related to the distribution of the final state leptons decayed from the (anti-)top quark. Based on the $t\bar{t}$ spin correlations, the observables related to the $t\bar{t}H$ interaction can be defined as

$$
\begin{aligned}
O_1 &= \hat{q}_+ \cdot \hat{q}_-, \\
O_2 &= (\hat{q}_+ \cdot \hat{k}_t)(\hat{q}_- \cdot \hat{k}_{\bar{t}}), \\
O_3 &= (\hat{q}_+ \cdot \hat{p})(\hat{q}_- \cdot \hat{p}), \\
O_4 &= (\hat{k}_t - \hat{k}_{\bar{t}}) \cdot (\hat{q}_+ \times \hat{q}_-).
\end{aligned}
$$

where $\hat{q}_+$ ($\hat{q}_-$) is the unit vector of the l^+ (l^-) direction of motion in the top (anti-top) quark rest frame, $\hat{k}_t(\hat{k}_{\bar{t}})$ is the unit vector of the $t(\bar{t})$ direction of motion in the rest frame, and $\hat{p}$ is the unit vector of the $t\bar{t}H$ system direction of motion in the pp rest frame. O_4 is a parity violated observable which is sensitive to parity violated interactions. It is proportional to the interference term between scalar and pseudoscalar components. Therefore it will disappear for a pure scalar or pure pseudoscalar Higgs.

For the numerical results, we define the expectation value of the operator as

$$
\langle O_i \rangle = \frac{\int O_i \mathrm{d}\sigma}{\int \mathrm{d}\sigma}, \qquad (i = 1,2,3,4), \tag{7}
$$

where σ is the cross section of process (6). $\langle O_i \rangle$ can be obtained from equation (5). One can find that

$$
\begin{aligned}
&\langle O_1 \rangle = -D/3, \\
&\langle O_2 \rangle = -A_3/9, && \text{with } \hat{a} = \hat{k}_t, \hat{b} = \hat{k}_{\bar{t}}, \\
&\langle O_3 \rangle = -A_3/9, && \text{with } \hat{a} = \hat{b} = \hat{p}, \\
&\langle O_4 \rangle = (A_1 - A_2)/3, && \text{with } \hat{a} = \hat{k}_t \times \hat{q}_-, \\
& && \hat{b} = \hat{k}_{\bar{t}} \times \hat{q}_+.
\end{aligned}
$$

In Table 1 we display the observables at the collision energies of 13 TeV and 33 TeV at the LHC. The gluon fusion and quark pair annihilation subprocesses contribute opposite signs for the observables in the $t\bar{t}H$ production, which is the same as in the $t\bar{t}$ production [23].

Table 1. Observables at the LHC 13 TeV and 33 TeV for $m_{\rm H}=125$ GeV.

	13 TeV			33 TeV		
	$\langle O_1\rangle$	$\langle O_2\rangle$	$\langle O_3\rangle$	$\langle O_1\rangle$	$\langle O_2\rangle$	$\langle O_3\rangle$
$q\bar{q}$	−0.0354	0.0077	−0.0362	−0.0167	0.0035	−0.0169
gg	0.0861	−0.0304	0.0172	0.0979	−0.0365	0.0177
total	0.0507	−0.0227	−0.0190	0.0812	−0.0330	0.0008

3.2 Heavy Higgs production associated with $t\bar{t}$

It is possible for a scalar heavy Higgs production to be associated with the top quark pair. From the Lagrangian of (3), it can be found that the form of the heavy Higgs boson coupling to the top quark is the same as the Higgs boson in the SM. On the condition of $\epsilon^{t}_{H_2}=1$, the cross sections of process (6) as a function of center-of-mass energy for different Higgs masses are displayed in Fig. 3. The heavy Higgs properties can be investigated at a high collision energy or with a high luminosity.

We display the contributions from the gg and $q\bar{q}$ sub-processes for $\langle O_1\rangle$, $\langle O_2\rangle$ and $\langle O_3\rangle$ with respect to various Higgs masses at LHC 13 TeV in Fig. 4. For $\langle O_1\rangle$ and $\langle O_3\rangle$ the contributions of these two sub-processes have different signs. The contribution from the gluon fusion process descends with the Higgs mass increasing for $\langle O_1\rangle$, while it increases for $\langle O_2\rangle$ and $\langle O_3\rangle$. The contribution from the quark annihilation process descends with the Higgs mass increasing for $\langle O_2\rangle$, while it increases for $\langle O_1\rangle$ and $\langle O_3\rangle$. The difference is from the dynamic effects. When the mass of Higgs is larger than 250 GeV, the contributions for $\langle O_2\rangle$ from gg and $q\bar{q}$ are the same sign. So the spin observables are related to the Higgs mass. As an example, we list the results of the spin observables in Table 2 with the Higgs mass of 500 GeV at the LHC 13 TeV and 33 TeV.

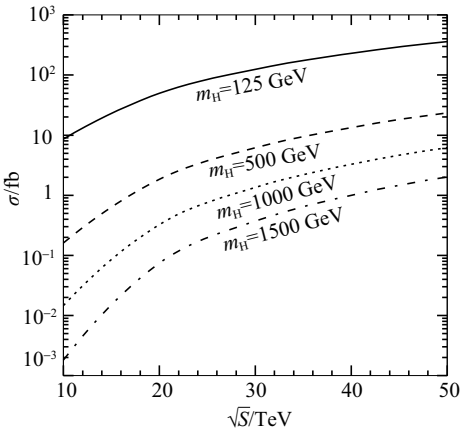

Fig. 3. The cross sections for process (6) as a function of center-of-mass energy for different scalar Higgs masses.

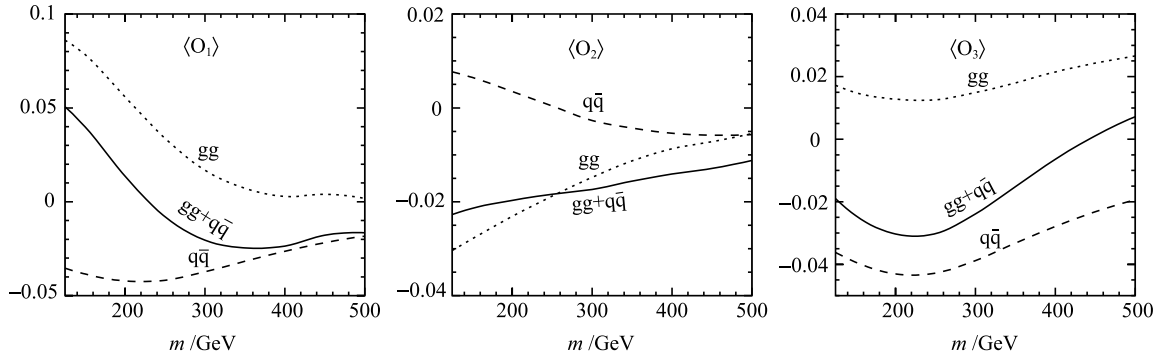

Fig. 4. The observables of process (6) at the LHC 13 TeV as a function of mass of the Higgs boson.

Table 2. Observables at the LHC 13 TeV and 33 TeV for $m_{\rm H}=500$ GeV.

	13 TeV			33 TeV		
	$\langle O_1\rangle$	$\langle O_2\rangle$	$\langle O_3\rangle$	$\langle O_1\rangle$	$\langle O_2\rangle$	$\langle O_3\rangle$
$q\bar{q}$	−0.0183	−0.0058	−0.0195	−0.0059	−0.0024	−0.0064
gg	0.0036	−0.0054	0.0267	0.0090	−0.0077	0.0227
total	−0.0147	−0.0112	0.0072	0.0031	−0.0101	0.0163

3.3 Scalar-pseudoscalar mixing Higgs production associated with $t\bar{t}$

A toy model can be used to illustrate the CP properties of the Higgs boson. Supposing that the light CP-even and CP-odd Higgs bosons are mass degenerate in the Two Higgs Doublet Models, one can write the interaction between the light Higgs and top quark pair in a general formula as follows,

$$\mathcal{L}_{t\bar{t}H}=-\frac{m_t}{v}(\epsilon^{t}_{H_1}-i\epsilon^{t}_{A}\gamma_5)t\bar{t}H, \quad (8)$$

where $\epsilon^{t}_{H_1}=\cos\alpha/\sin\beta$ and $\epsilon^{t}_{A}=\cot\beta$ with α the mixing angle of the scalar fields. For our numerical results we choose the corresponding values of α and β as in Table 3 and $m_{\rm H}=125$ GeV as an example. $\alpha=0$ and $\beta=\pi/2$ corresponds to the SM-Higgs, and $\alpha=\pi/2$ and $\beta=\pi/4$ to the pseudoscalar Higgs (A). The other two cases correspond to the scalar-pseudoscalar mixing Higgs. The cor-

responding cross sections of process (6) at the hadron collider are displayed in Fig. 5 with different $t\bar{t}H$ couplings. The normalized differential distributions of $\sigma^{-1}d\sigma/dM_{t\bar{t}}$ are changed with various $t\bar{t}H$ couplings. The normalized differential distributions of $\sigma^{-1}d\sigma/dO_i$ (i=1,2,3,4) for process (6) at the LHC 13 TeV are plotted in Fig. 6. These differential distributions with observables can be distinguished from different models.

Table 3. Parameters set in the numerical calculations.

α	0	$\pi/2$	$\pi/4$	$\pi/3$
β	$\pi/2$	$\pi/4$	$\pi/4$	$\pi/6$
$\epsilon^t_{H_1}$	1	0	1	1
ϵ^t_A	0	1	1	$\sqrt{3}$

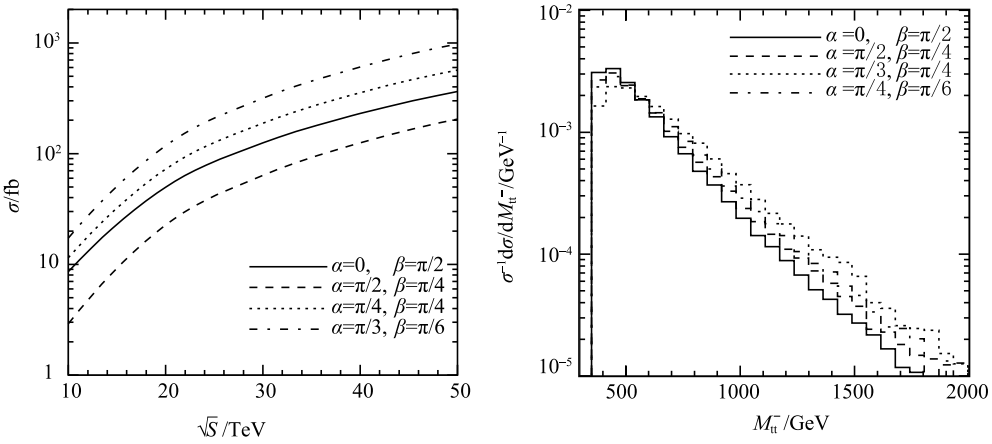

Fig. 5. (a) The cross sections for process (6) as a function of center-of-mass energy with Higgs mass 125 GeV; (b) The normalized differential distribution as a function of invariant mass of $t\bar{t}$ at the LHC 13 TeV (right).

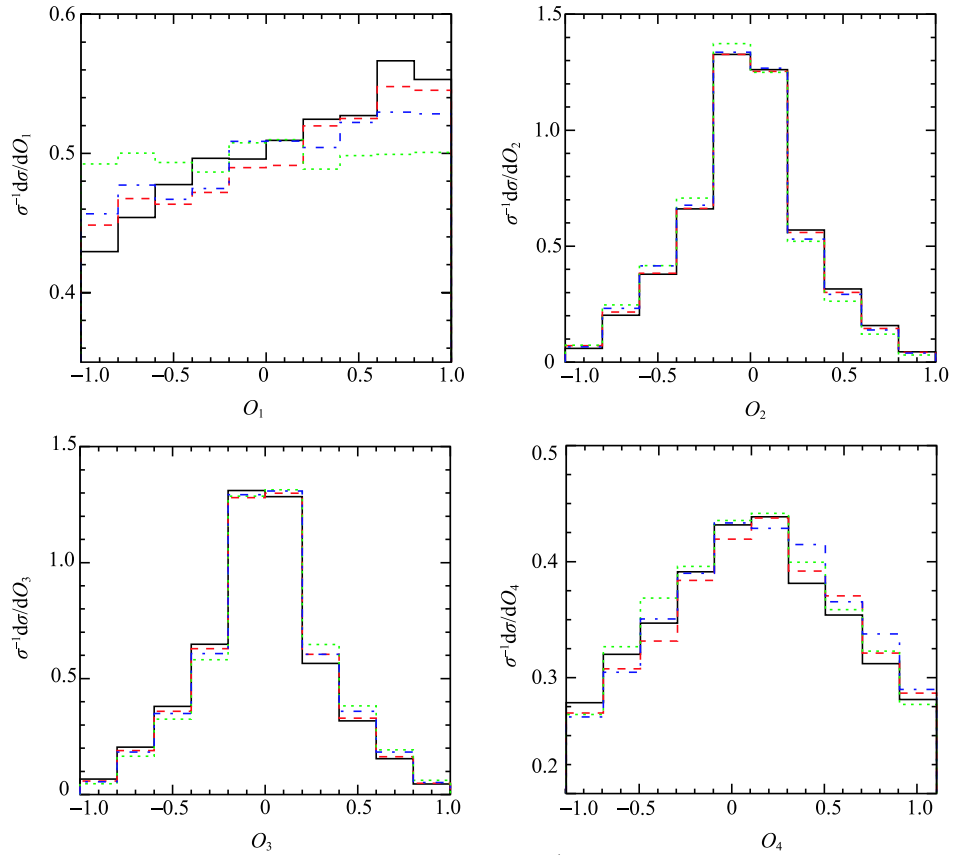

Fig. 6. (color online) Normalized differential distribution of $\sigma^{-1}d\sigma/dO_i$ (i=1,2,3,4) for process (6) at the LHC 13 TeV. The solid (black) line stands for $\alpha=0,\beta=\pi/2$. The dotted (green) line stands for $\alpha=\pi/2,\beta=\pi/4$. The dashed (red) line stands for $\alpha=\pi/4,\beta=\pi/4$. The dash-dotted (blue) line stands for $\alpha=\pi/3,\beta=\pi/6$.

The observables corresponding to process (6) at the LHC are listed in Tables 4 and 5 for the collision energies of 13 and 33 TeV. The values of these observables are different in the scalar, pseudoscalar and scalar-pseudoscalar mixing Higgs production. The gluon fusion and the quark pair annihilation sub-processes contribute the same sign for the observables $\langle O_2\rangle$ and $\langle O_3\rangle$ from pseudoscalar Higgs production, which differs from the scalar Higgs production. It is found that $\langle O_4\rangle$ is a characteristic quantity to distinguish the scalar-pseudoscalar mixing Higgs from the pure scalar and the pseudoscalar Higgs. In addition, the distributions of $\langle O_1\rangle$ as functions of $t\bar{t}$ invariant mass are displayed in Fig. 7. The shapes of the distribution can be used to distinguish the different models. So the precision measurement of these observables will be helpful to study the $t\bar{t}H$ interaction and the properties of the Higgs. aMC@NLO can handle the spin correlation in $t\bar{t}H$ production at the LHC [55]. The NLO effect is about 50% for $\langle O_1\rangle$. However, this only includes the spin correlation effects at tree-level accuracy, so the information from the virtual amplitudes is not included.

Table 4. Observables at the LHC 13 TeV for Higgs mass 125 GeV.

α	β	$q\bar{q}$	gg	total
$\pi/2$	$\pi/4$	−0.0037	0.0092	0.0055
$\pi/4$	$\pi/4$	−0.0267	0.0650	0.0383
$\pi/3$	$\pi/6$	−0.0185	0.0451	0.0266

(a) $\langle O_1\rangle$

α	β	$q\bar{q}$	gg	total
$\pi/2$	$\pi/4$	−0.0089	−0.0436	−0.0525
$\pi/4$	$\pi/4$	0.0031	−0.0340	−0.0309
$\pi/3$	$\pi/6$	−0.0012	−0.0374	−0.0386

(b) $\langle O_2\rangle$

α	β	$q\bar{q}$	gg	total
$\pi/2$	$\pi/4$	0.0025	0.0138	0.0163
$\pi/4$	$\pi/4$	−0.0253	0.0160	−0.0093
$\pi/3$	$\pi/6$	−0.0153	0.0153	0

(c) $\langle O_3\rangle$

α	β	$q\bar{q}$	gg	total
$\pi/2$	$\pi/4$	0	0	0
$\pi/4$	$\pi/4$	−0.0104	0.0437	0.0333
$\pi/3$	$\pi/6$	−0.0116	0.0484	0.0368

(d) $\langle O_4\rangle$

Table 5. Observables at the LHC 33 TeV for Higgs mass 125 GeV.

α	β	$q\bar{q}$	gg	total
$\pi/2$	$\pi/4$	−0.0013	0.0097	0.0084
$\pi/4$	$\pi/4$	−0.0114	0.0674	0.0560
$\pi/3$	$\pi/6$	−0.0073	0.0439	0.0366

(a) $\langle O_1\rangle$

α	β	$q\bar{q}$	gg	total
$\pi/2$	$\pi/4$	−0.0035	−0.0445	−0.0480
$\pi/4$	$\pi/4$	0.0011	−0.0392	−0.0381
$\pi/3$	$\pi/6$	−0.0008	−0.0414	−0.0422

(b) $\langle O_2\rangle$

α	β	$q\bar{q}$	gg	total
$\pi/2$	$\pi/4$	0.0010	0.0127	0.0137
$\pi/4$	$\pi/4$	−0.0107	0.0159	0.0052
$\pi/3$	$\pi/6$	−0.0060	0.0146	0.0086

(c) $\langle O_3\rangle$

α	β	$q\bar{q}$	gg	total
$\pi/2$	$\pi/4$	0	0	0
$\pi/4$	$\pi/4$	−0.0045	0.0498	0.0453
$\pi/3$	$\pi/6$	−0.0046	0.0510	0.0464

(d) $\langle O_4\rangle$

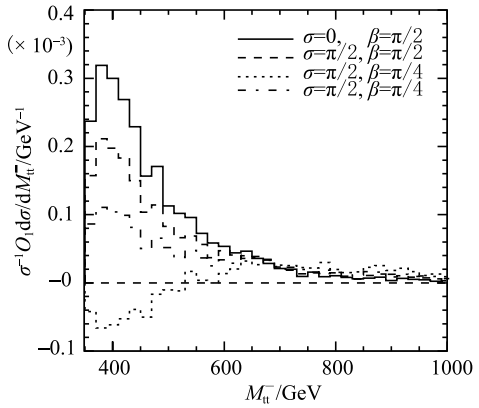

Fig. 7. The differential distribution of $\sigma^{-1}O_1\mathrm{d}\sigma/\mathrm{d}M_{t\bar{t}}$ with the invariant mass of $t\bar{t}$ at the LHC 13 TeV.

3.4 Signal and backgrounds at the LHC

To get an idea of the sensitivity one must include backgrounds. For the signal of $pp\to t\bar{t}H\to b\bar{b}l^+l^-\nu_l\bar{\nu}_l+b\bar{b}$, the detector signal for the process we investigate will be two leptons, four b-jets and missing energy. The main backgrounds with the same collider signal are

$$\begin{aligned} &pp\to t\bar{t}jj\\ &pp\to t\bar{t}b\bar{b}\\ &pp\to t\bar{t}Z\to t\bar{t}b\bar{b}, \end{aligned} \tag{9}$$

where j stands for a light jet. According to the analysis in Ref. [56], the top quark can be reconstructed by solving the kinematic equations obtained when imposing energy-momentum conservation at each of the decay

vertices of the process. From the leptonic decay channel, the top quark reconstruction efficiency can be up to 80%. The reconstruction details can be found in Ref. [49].

To highlight the signal process from the backgrounds, we set the kinematics cuts as

$$\begin{cases} P_{\rm T} \geqslant 20 \text{ GeV} \\ |y| \leqslant 3.0 \end{cases}, \tag{10}$$

where $P_{\rm T}$ is the transverse momentum of the charged leptons and the b-jets, and y is the corresponding rapidity. The differences of the signal and the background processes are mostly from the remaining two jets that are not used to reconstruct the top and anti-top quarks, thus we require the invariant mass of these two jets to be close to the Higgs mass, i.e.,

$$|M_{\rm jj} - M_{\rm H}| \leqslant 0.1 M_{\rm H}. \tag{11}$$

We simulate the backgrounds processes by the MADGRAPH program [57], where sets of accepted cuts are used. The results are summarized in Table 6. The backgrounds are three orders of magnitude larger than the signal process before cuts, while this gap disappears after the cuts. For the SM-like Higgs boson production at LHC 13 TeV, the significance can be up to $S/B = 0.3$ and $S/\sqrt{B} = 10.1$ for an integrated luminosity of 300 fb^{-1}. When the collision energy is up to 33 TeV, the heavy Higgs with a mass of 500 GeV can be detected with a signal-to-background ratio $S/B = 0.07$ and significance $S/\sqrt{B} = 5.79$ for an integrated luminosity of 1000 fb^{-1}.

Table 6. Summary of the cross sections (fb) for the signal and background processes at the LHC 13 TeV with an integrated luminosity of 300 fb^{-1} and 33 TeV with an integrated luminosity of 1000 fb^{-1} before and after cuts. The significances are listed in the last two columns.

$\sqrt{S}$	$m_{\rm H}$ /GeV	before cut		after cut			
		signal	backgrounds	signal	backgrounds	S/B	$S/\sqrt{B}$
13 TeV	125	2.05	8039.7	1.14	3.81	0.30	10.1
	500	0.051		0.031	0.43	0.07	0.82
33 TeV	125	18.02	1.24×10^5	9.86	44.2	0.22	46.9
	500	0.65		0.49	7.16	0.07	5.79

4 Summary

A large number of Higgs events will be accumulated at the LHC, and the properties of Higgs boson should be investigated. In the SM, one CP-even Higgs boson is assumed via the simplest scalar doublet, which could be naturally extended in the new physics models, such as the Two Higgs Doublet Models. The phenomenology of the Higgs sector is extremely rich, since it contains more than one Higgs. The interactions of Higgs boson coupling to other particles are more complex than those in the SM. Therefore, to discriminate the new physics models, it is important to study the properties of the Higgs. For this aim, in this paper we study $t\bar{t}H$ production and its related spin effects at the LHC. The top quark spin correlation, reflected by the motion of the particles decaying from the top quark pair, is related to the dynamics of $t\bar{t}H$ production. These spin correlations are related to the couplings of the $t\bar{t}H$ interaction and the Higgs mass. To study these spin effects, we use the observables $\langle O_i \rangle$ $(i = 1,2,3,4)$ to investigate the properties of the scalar, pseudoscalar and scalar-pseudoscalar mixing Higgs in $t\bar{t}H$ production. With the large number of $t\bar{t}H$ events at the LHC, the Higgs properties can be clarified so that the new physics models can be discriminated.

References

1 G. Aad et al(ATLAS Collaboration), Phys. Lett. B, **716**: 1 (2012)
2 S. Chatrchyan et al(CMS Collaboration), Phys. Lett. B, **716**: 30 (2012)
3 G. Aad et al(ATLAS Collaboration), Phys. Rev. D, **90**: 052004 (2014)
4 S. Chatrchyan et al(CMS Collaboration), Eur. Phys. J. C, **75**: 212 (2015)
5 G. Aad et al(ATLAS Collaboration), Phys. Lett. B, **726**: 120 (2013)
6 S. Chatrchyan et al(CMS Collaboration), Phys. Rev. D, **92**: 012004 (2015)
7 G. Aad et al(ATLAS Collaboration), ATLAS-CONF-2014-009
8 T. D. Lee, Phys. Rev. D, **8**: 1226 (1973)
9 S. Weinberg, Phys. Rev. Lett., **37**: 657 (1976)
10 J. Liu and L. Wolfenstein, Nucl. Phys. B, **289**: 1 (1987)
11 J. Wess, and B. Zumino, Phys. Lett. B, **49**: 52 (1974)
12 H. E. Haber and G. L. Kane, Phys. Rept., **117**: 75 (1985)
13 S. P. Martin, Adv. Ser. Direct. High Energy Phys., **21**: 1 (2010)
14 J. C. Pati and A. Salam, Phys. Rev. D, **10**: 275 (1974)
15 R. N. Mohapatra and J. C. Pati, Phys. Rev. D, **11**: 566 (1975)
16 R. N. Mohapatra and J. C. Pati, Phys. Rev. D, **11**: 2558 (1975)
17 G. Senjanovic and R. N. Mohapatra, Phys. Rev. D, **12**: 1502 (1975)
18 R. N. Mohapatra, F. E. Paige, and D. P. Sidhu, Phys. Rev. D,

17: 2462 (1978)
19 W. Bernreuther, A. Brandenburg, Z. G. Si, and P. Uwer, arXiv:hep-ph/0410197
20 W. Bernreuther and Z. G. Si, Nucl. Phys. B, **837**: 90 (2010)
21 W. Bernreuther and Z. G. Si, Phys. Rev. D, **86**: 034026 (2012)
22 J. A. Aguilar-Saavedra, W. Bernreuther, and Z. G. Si, Phys. Rev. D, **86**: 115020 (2012)
23 W. Bernreuther, A. Brandenburg, Z. G. Si, and P. Uwer, Nucl. Phys. B, **690**: 81 (2004)
24 W. Bernreuther, A. Brandenburg, and Z. G. Si, Phys. Lett. B, **483**: 99 (2000)
25 W. Bernreuther, A. Brandenburg, Z. G. Si, and P. Uwer, Nucl. Phys. Proc. Suppl., **117**: 294 (2003)
26 A. Brandenburg, Z. G. Si, and P. Uwer, Phys. Lett. B, **539**: 235 (2002)
27 W. Bernreuther, A. Brandenburg, Z. G. Si, and P. Uwer, Phys. Rev. Lett., **87**: 242002 (2001)
28 W. Bernreuther, A. Brandenburg, Z. G. Si, and P. Uwer, Phys. Lett. B, **509**: 53 (2001)
29 S. Gopalakrishna and T. Han, I. Lewis et al, Phys. Rev. D, **82**: 115020 (2010)
30 X. Gong, Z. G. Si, S. Yang, and Y. J. Zheng, Phys. Rev. D, **87**: 035014 (2013)
31 W. Bernreuther and Z. G. Si, Phys. Lett. B, **725**: 115 (2013)
32 Z. Kunszt, Nucl. Phys. B, **247**: 339 (1984)
33 W. J. Marciano and F. E. Paige, Phys. Rev. Lett., **66**: 2433 (1991)
34 S. Dawson, L. H. Orr, L. Reina, and D. Wackeroth, Phys. Rev. D, **67**: 071503 (2003)
35 W. Beenakker, S. Dittmaier, M. Kramer et al, Phys. Rev. Lett., **87**: 201805 (2001)
36 W. Beenakker, S. Dittmaier, M. Kramer et al, Nucl. Phys. B, **653**: 151 (2003)
37 S. Dawson and L. Reina, Phys. Rev. D, **57**: 5851 (1998)
38 S. Dittmaier et al(LHC Higgs Cross Section Working Group Collaboration), arXiv:1101.0593
39 G. Aad et al(ATLAS Collaboration), ATLAS-CONF-2014-011
40 V. Khachatryan et al(CMS Collaboration), Eur. Phys. J. C, **75**: 251 (2015)
41 D. Curtin, J. Galloway, and J. G. Wacker, Phys. Rev. D, **88**: 093006 (2013)
42 CMS Collaboration(CMS Collaboration), JHEP, **1409**: 087 (2014)
43 K. Nishiwaki, S. Niyogi, and A. Shivaji, JHEP, **1404**: 011 (2014)
44 F. Maltoni, D. L. Rainwater, and S. Willenbrock, Phys. Rev. D, **66**: 034022 (2002)
45 S. Biswas, R. Frederix, E. Gabrielli, and B. Mele, JHEP, **1407**: 020 (2014)
46 X. G. He, G. N. Li, and Y. J. Zheng, Int. J. Mod. Phys. A, **30**: 1550156 (2015)
47 M. R. Buckley and D. Goncalves, arXiv:1507.07926
48 M. R. Buckley, T. Plehn, T. Schell, and M. Takeuchi, JHEP, **1402**: 130 (2014)
49 S. P. Amor dos Santos et al, Phys. Rev. D, **92**: 034021 (2015)
50 R. Frederix, S. Frixione, V. Hirschi et al, Phys. Lett. B, **701**: 427 (2011)
51 J. Ellis, D. S. Hwang, K. Sakurai, and M. Takeuchi, JHEP, **1404**: 004 (2014)
52 F. Demartin, F. Maltoni, K. Mawatari et al, Eur. Phys. J. , **74**: 3065 (2014)
53 F. Boudjema, R. M. Godbole, D. Guadagnoli, and K. A. Mohan, Phys. Rev. D, **92**: 015019 (2015)
54 S. Khatibi, and M. M. Najafabadi, Phys. Rev. D, **90**: 074014 (2014)
55 P. Artoisenet, R. Frederix, O. Mattelaer, and R. Rietkerk, JHEP, **1303**: 015 (2013)
56 G. Aad et al(ATLAS Collaboration), JHEP, **05**: 061 (2015)
57 J. Alwall, R. Frederix, S. Frixione et al, JHEP, **1407**: 079 (2014)